J. Fluid Mech. (2008), *vol.* 600, *pp.* 77–94. © 2008 Cambridge University Press
doi:10.1017/S0022112008000359 Printed in the United Kingdom

Stability of a coupled body–vortex system

EVA KANSO AND BABAK GHAEMI OSKOUEI
University of Southern California, Los Angeles, CA 90089, USA

(Received 11 August 2007 and in revised form 26 October 2007)

This paper considers the dynamics of a rigid body interacting with point vortices in a perfect fluid. The fluid velocity is obtained using the classical complex variables theory and conformal transformations. The equations of motion of the solid–fluid system are formulated in terms of the solid variables and the position of the point vortices only. These equations are applied to study the dynamic interaction of an elliptic cylinder with vortex pairs because of its relevance to understanding the swimming of fish in an ambient vorticity field. Two families of relative equilibria are found: moving Föppl equilibria; and equilibria along the ellipse's axis of symmetry (the axis perpendicular to the direction of motion). The two families of relative equilibria are similar to those present in the classical problem of flow past a fixed body, but their stability differs significantly from the classical ones.

1. Introduction

This paper is concerned with the dynamics and stability of a rigid body interacting with point vortices in potential flow. The primary motivation is to study the interaction of fish with ambient vorticity. Liao *et al.* (2003) have reported that live rainbow trout exploit the vortices in the ambient flow to reduce their locomotory costs, taking advantage of the vortex energy in the surrounding fluid. Beal *et al.* (2006) showed that dead trout can recover sufficient energy from the surrounding flow to allow it to swim passively upstream. Inspired by these results, we propose a reduced model of a rigid body interacting dynamically with surrounding point vortices and we demonstrate that the rigid body can swim in the direction opposite to the motion of point vortices at no energy cost. Indeed, the rigid body itself does not generate any force and its motion is due entirely to energy available from the presence of the point vortices.

The dynamics of a rigid body interacting with point vortices was considered in Borisov & Mamaev (2003) and in Shashikanth *et al.* (2002) and Shashikanth (2005) for the case when the vortex strength sum to zero ($\sum_{k=1}^{N} \Gamma_k = 0$). The equations governing the motion of the rigid body were derived using Newtonian mechanics while the motion of the point vortices was described by a Kirchhoff–Routh function. The resulting equations were shown to have a Hamiltonian structure and were applied to the study of a circular cylinder. In this work, we appeal to the classical theory of complex variables and conformal transformations to generalize the results in Shashikanth *et al.* (2002) and Shashikanth (2005) to a cylinder of any cross-sectional geometry (that can be mapped conformally to a unit circle). More specifically, we generalize the results of Lin (1941*a*, *b*) concerning the motion of N point vortices in a multiply connected fluid domain with fixed boundaries where he established the existence of a *Kirchhoff–Routh function* governing the motion of the vortices and investigated its behaviour under conformal transformations of the fluid motion. We derive the equations of motion when the net circulation around the moving

https://doi.org/10.1017/S0022112008000359 Published online by Cambridge University Press

cylinder does not necessarily sum to zero. Note that the governing equations were simultaneously derived in Borisov, Mamaev & Ramodanov (2007) following a different approach with emphasis on the Hamiltonian structure of the system. Also note that the interactions of multiple rigid bodies in potential flow was considered in Wang (2004), Kanso *et al.* (2005), Crowdy, Surana & Yick (2007) and Nair & Kanso (2007).

We use the derived equations to study the motion of an elliptic cylinder interacting with a vortex pair for its relevance to understanding the swimming of fish in an ambient vorticity field. We examine the stability of the relative equilibria of the vortex–ellipse system. By relative equilibria, we mean motions where the vortex pair and the elliptic cylinder move rigidly (at the same velocity). We find two families of such equilibria. The first family is a generalization of the classical Föppl equilibria behind a stationary circular cylinder in an ambient uniform flow and was discussed in Shashikanth *et al.* (2002) for the case of a moving circular cylinder. The second family of equilibria is located at the ellipse's axis of symmetry which is perpendicular to the direction of motion. Both families of equilibria are observed in the classical problem of flow past a stationary ellipse (see e.g. Hill 1998). However, the stability of the relative equilibria of the moving ellipse–vortex system differs significantly from the stability of the classical equilibria for flow past a stationary ellipse. In the classical problem, we find, subject to symmetric perturbations, that the Föppl equilibria are stable and the equilibria along the axis of symmetry are unstable. For an ellipse interacting dynamically with a vortex pair, the Föppl equilibria are mostly unstable subject to symmetric perturbations whereas the equilibria along the ellipse's axis of symmetry are mostly stable subject to such perturbations. These unstable and stable equilibria may be important for designing the swimming motion of the solid body. We explore this idea via numerical examples.

The organization of this paper is as follows. The problem setting is described in § 2. The fluid velocity is discussed in § 3. The streamfunction which dictates the fluid velocity is obtained in § 4 using conformal transformation. The equations governing the motion of the solid body are derived in § 5 using Newtonian mechanics. The problem of an elliptic body interacting with vortex pairs is considered in § 6. The findings of this work and future directions are summarized in § 7.

2. Problem setting

Consider a planar body moving in an infinitely large volume of incompressible, inviscid and irrotational fluid $\mathscr{F}$ at rest at infinity. The body $\mathscr{B}$ is assumed to occupy a simply connected region whose boundary can be conformally mapped to a unit circle, and it is considered to be uniform neutrally-buoyant (the body weight is balanced by the force of buoyancy). Introduce an orthonormal inertial frame $\{\boldsymbol{e}_{1,2,3}\}$ where $\{\boldsymbol{e}_1, \boldsymbol{e}_2\}$ span the plane of motion and $\boldsymbol{e}_3$ is the unit normal to this plane. The configuration of the submerged rigid body can then be described by a rotation β about $\boldsymbol{e}_3$ and a translation $\boldsymbol{x}_o = x_o\boldsymbol{e}_1 + y_o\boldsymbol{e}_2$ of a point O (often chosen to coincide with the mass centre) in the $\{\boldsymbol{e}_1, \boldsymbol{e}_2\}$ directions. The angular and translational velocities expressed relative to the inertial frame are of the form $\dot{\beta}\,\boldsymbol{e}_3$ and $\boldsymbol{v} = v_x\,\boldsymbol{e}_1 + v_y\,\boldsymbol{e}_2$ where $v_x = \dot{x}_o$, $v_y = \dot{y}_o$ (the dot denotes derivative with respect to time t). It is convenient for the following development to introduce a moving frame $\{\boldsymbol{b}_{1,2,3}\}$ attached to the body. The point transformation from the body to the inertial frame can be represented as

$$\boldsymbol{x} = R\boldsymbol{X} + \boldsymbol{x}_o, \qquad R = \begin{pmatrix} \cos\beta & -\sin\beta \\ \sin\beta & \cos\beta \end{pmatrix}, \tag{1}$$

https://doi.org/10.1017/S0022112008000359 Published online by Cambridge University Press

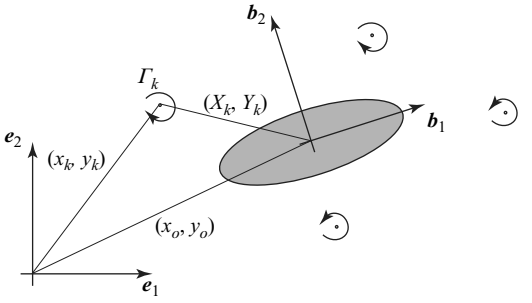


FIGURE 1. A rigid body undergoing a general rigid motion and interacting with N point vortices.

where $\boldsymbol{x} = x\,\boldsymbol{e}_1 + y\,\boldsymbol{e}_2$ and $\boldsymbol{X} = X\,\boldsymbol{b}_1 + Y\,\boldsymbol{b}_2$, while vectors transform as $\boldsymbol{v} = R\boldsymbol{V}$. The angular and translational velocities expressed in the body frame take the form $\boldsymbol{\Omega} = \Omega\,\boldsymbol{b}_3$ (where $\Omega = \dot{\beta}$) and $\boldsymbol{V} = V_1\boldsymbol{b}_1 + V_2\boldsymbol{b}_2$ (where $V_1 = \dot{x}_o\cos\beta + \dot{y}_o\sin\beta$ and $V_2 = -\dot{x}_o\sin\beta + \dot{y}_o\cos\beta$).

Let N point vortices of strength Γ_k $(k = 1, \ldots, N)$ be placed in the fluid domain which extends to infinity and is bounded internally by the rigid body. The positions of the point vortices are denoted by (x_k, y_k) in the inertial frame $\{\boldsymbol{e}_i\}$ and (X_k, Y_k) in the body frame $\{\boldsymbol{b}_i\}$. In this work, we take Γ_k to be positive in the counterclockwise direction, and we do not require the sum $\sum_{k=1}^{n}\Gamma_k$ of strength of the point vortices nor the net circulation Γ_o around the rigid body to be zero (figure 1).

3. Fluid velocity

The fluid velocity $\boldsymbol{u} = u_x\boldsymbol{e}_1 + u_y\boldsymbol{e}_2$ at a point (x, y) that does not coincide with a point vortex is given by the real potential function ϕ or the streamfunction ψ

$$(u_x, u_y) = \left(\frac{\partial\phi}{\partial x}, \frac{\partial\phi}{\partial y}\right), \quad \text{or, alternativerly, } (u_x, u_y) = \left(\frac{\partial\psi}{\partial y}, -\frac{\partial\psi}{\partial x}\right). \tag{2}$$

The existence of ϕ and ψ are guaranteed by irrotationality and by the continuity equation $\mathrm{div}(\boldsymbol{u}) = 0$, respectively. From the linearity of the problem, the streamfunction $\psi(x, y)$ can be written in the form

$$\psi = \psi^b + \psi^v + \Gamma_o\psi_o. \tag{3}$$

Similarly, we may write $\phi = \phi^b + \phi^v + \Gamma_o\phi_o$. The streamfunction ψ^b is due to the motion of the solid body. It may be written in the Kirchhoff form (see e.g. Lamb 1932)

$$\psi^b = \psi_x v_x + \psi_y v_y + \psi_\beta\dot{\beta}. \tag{4}$$

Here, ψ_x, ψ_y and ψ_β are harmonic functions in the fluid domain $\mathscr{F}$ subject to the boundary conditions

$$\psi^b|_{\partial\mathscr{B}} = yv_x - xv_y + \tfrac{1}{2}((x - x_o)^2 + (y - y_o)^2)\dot{\beta}, \qquad \psi^b|_\infty = 0. \tag{5}$$

Similarly, we have

$$\phi^b = \varphi_x v_x + \varphi_y v_y + \varphi_\beta\dot{\beta}, \tag{6}$$

https://doi.org/10.1017/S0022112008000359 Published online by Cambridge University Press

where φ_x, φ_y and φ_β are harmonic functions subject to the boundary conditions

$$\left.\frac{\partial \phi^b}{\partial n}\right|_{\partial \mathscr{B}} = n_x v_x + n_y v_y + ((x-x_o)n_y - (y-y_o)n_x)\dot{\beta}, \qquad \phi^b|_\infty = 0, \tag{7}$$

where (n_x, n_y) are the components of the unit normal $\boldsymbol{n} = n_x \boldsymbol{e}_1 + n_y \boldsymbol{e}_2$ into the fluid.

The streamfunction ψ^v due to the presence of the point vortices satisfies

$$\Delta \psi^v = -\sum_k \Gamma_k \delta(x-x_k)\delta(y-y_k), \tag{8}$$

where $\delta(x-x_k)$ and $\delta(y-y_k)$ denote the Dirac delta function. ψ^v can be written as

$$\psi^v = \sum_k \Gamma_k \psi_k, \tag{9}$$

where ψ_k are harmonic everywhere in the fluid domain $\mathscr{F}$ except at the kth vortex and they satisfy the boundary conditions

$$\psi_k|_{\partial \mathscr{B}} = \text{constant}, \qquad \psi_k|_\infty = 0. \tag{10}$$

Lastly, $\Gamma_o \psi_o$ represents the streamfunctions due to a non-zero net circulatory flow around the body. Here, ψ_o is harmonic in the fluid domain satisfying the boundary conditions

$$\psi_o|_{\partial \mathscr{B}} = \text{constant}, \qquad \psi_o|_\infty = 0\ . \tag{11}$$

The quantity Γ_o can be interpreted as follows. Assume a non-zero constant circulation Γ_c around the body that may be caused by the presence of the point vortices as well as the presence of a pure circulatory flow around the body (that does not vanish when vortex strength Γ_k are set to zero). The circulation Γ_c is defined as

$$\Gamma_c = \oint_{\partial \mathscr{B}} \boldsymbol{u} \cdot \mathrm{d}\boldsymbol{x} = \oint_{\partial \mathscr{B}} \frac{\partial \psi}{\partial n}\, \mathrm{d}s = \sum_k \Gamma_k + \Gamma_o. \tag{12}$$

Clearly, Γ_o represents the total circulation around the body minus the circulation induced by the point vortices.

4. Streamfunction, Kirchhoff–Routh function and vortex motion

The streamfunction ψ can be calculated using a *conformal transformation* that relates the flow field in the region exterior to the body to that in the region exterior to the unit circle. For concreteness, let the rigid body be placed in the plane parameterized by (x, y) and let a circle of unit radius be placed in a plane parameterized by $(\tilde{x}, \tilde{y})$. It is more convenient for what follows to introduce the complex coordinates $\tilde{z} = \tilde{x} + \mathrm{i}\tilde{y}$ (where $\mathrm{i} = \sqrt{-1}$) and $z = x + \mathrm{i}y$, and their complex conjugates $\tilde{z}^* = \tilde{x} - \mathrm{i}\tilde{y}$ and $z^* = x - \mathrm{i}y$, respectively. To this end, the conformal transformation can be written as

$$\tilde{z} = F(z), \tag{13}$$

where the inverse transformation $\tilde{z} = F^{-1}(z)$ may be expanded into a Laurent series of the form (see e.g. Silverman 1974)

$$z = F^{-1}(\tilde{z}) = A\tilde{z} + z_o + \frac{A_1}{\tilde{z}} + \frac{A_2}{\tilde{z}^2} + \cdots, \qquad A, A_1, A_2, \ldots \in \mathbb{R}^+. \tag{14}$$

The point z_o is referred to as the conformal centre of the body. We assume that the origin of the body frame is placed at the conformal centre z_o. Note that we may

https://doi.org/10.1017/S0022112008000359 Published online by Cambridge University Press

rewrite the conformal transformation (13) in terms of body coordinates as $\tilde{Z} = F(Z)$ where $\tilde{Z} = \tilde{X} + \mathrm{i}\tilde{Y}$ is measured relative to a frame attached to the centre of the unit circle and $Z = X + \mathrm{i}Y$ is measured relative to the body frame attached to the conformal centre z_o.

The complex potential $w(z)$ is defined as $w(z) = \phi(x, y) + \mathrm{i}\psi(x, y)$ and the complex velocity $u = u_x + \mathrm{i}u_y$ (at a non-singular point) is given by $u^* = \mathrm{d}w/\mathrm{d}z$ (where u^* is the complex conjugate of u). The complex potential $w(z)$ in the z-plane is related to the complex streamfunction $\tilde{w}(\tilde{z})$ in the circle-plane by

$$w(z) = \tilde{w}(\tilde{z}) = \tilde{w}(F(z)). \tag{15}$$

Let $\omega^b = \phi^b + \mathrm{i}\psi^b$ be the complex potential due to the motion of the solid body with the harmonic functions ϕ^b and ψ^b subject to the boundary conditions (7) and (5), respectively. The problem of solving for ϕ^b and ψ^b can be restated as a Riemann–Hilbert problem of the form (see e.g. Muskhelishvili 1953; Crowdy *et al.* 2007)

$$\mathrm{Re}[-\mathrm{i}w^b(z)] = \mathrm{Re}\left[(v_x - \mathrm{i}v_y)(-\mathrm{i})(z - z_o) - \tfrac{1}{2}\dot{\beta}(z - z_o)^2\right] \qquad \text{on } \partial\mathscr{B}, \tag{16}$$

which can be transformed, using the conformal mapping (13) and its inverse, into a Dirichlet problem for the circle whose solution is given in terms of the Schwarz formula. It is more convenient for later to first express ϕ^b and ψ^b in terms of body coordinates: $\phi^b(X, Y) = V_1\,\varphi_1 + V_2\,\varphi_2 + \Omega\,\varphi_\Omega$ and $\psi^b(X, Y) = V_1\,\psi_1 + V_2\,\psi_2 + \Omega\,\psi_\Omega$ where $\phi_1, \phi_2, \phi_\Omega$ and $\psi_1, \psi_2, \psi_\Omega$ are functions of (X, Y) and are analogous to $\phi_x, \phi_y, \phi_\beta$ and $\psi_x, \psi_y, \psi_\beta$ of (6) and (4), respectively. To this end, (16) can be rewritten as

$$\mathrm{Re}\left[-\mathrm{i}w^b(Z)\right] = \mathrm{Re}\left[(V_1 - \mathrm{i}V_2)(-\mathrm{i}Z) - \tfrac{1}{2}\Omega Z^2\right] \qquad \text{on } \partial\mathscr{B}, \tag{17}$$

This equation becomes, under the conformal mapping to the circle plane,

$$\mathrm{Re}[-\mathrm{i}\tilde{w}^b(\tilde{Z})] = \mathrm{Re}\left[-\mathrm{i}(V_1 - \mathrm{i}V_2)(F^{-1}(\tilde{Z})) - \tfrac{1}{2}\Omega(F^{-1}(\tilde{Z}))^2\right] \qquad \text{on } |\tilde{Z}| = 1, \tag{18}$$

whose solution is given explicitly by the Schwarz formula

$$-\mathrm{i}\tilde{w}^b(\tilde{Z}) = \frac{1}{2\pi\mathrm{i}} \oint_{|\tilde{Z}'|=1} \mathrm{Re}\left[-\mathrm{i}(V_1 - \mathrm{i}V_2)(F^{-1}(\tilde{Z}')) - \tfrac{1}{2}\Omega(F^{-1}(\tilde{Z}'))^2\right] \frac{(\tilde{Z}' + \tilde{Z})}{(\tilde{Z}' - \tilde{Z})} \frac{\mathrm{d}\tilde{Z}'}{\tilde{Z}'} + \mathrm{i}C \tag{19}$$

where $\tilde{Z}'$ is the integration variable and C an arbitrary constant. The complex potential $w^b(Z) = \tilde{w}^b(F(Z))$ follows in a straightforward way. Note that this method can be readily generalized to the case of two or more interacting solids (see Muskhelishvili 1953; Crowdy *et al.* 2007).

The complex potential $\tilde{w}^v(\tilde{z})$ in the $\tilde{z}$-plane due to N point vortices located at $\tilde{z}_k$ outside the unit circle and of strength Γ_k is given by the well-known Milne-Thompson circle theorem

$$\tilde{w}^v(\tilde{z}) = \sum_k -\frac{\mathrm{i}\Gamma_k}{2\pi}\left[\log(\tilde{z} - \tilde{z}_k) - \log\left(\tilde{z} - \tilde{z}_k^I\right)\right], \tag{20}$$

where $\tilde{z}_k^I = \tilde{z}_o + 1/(\tilde{z}_k - \tilde{z}_o)^*$ denotes the position of image vorticity.

It is also known that the complex potential $\tilde{w}_o(\tilde{z})$ in the $\tilde{z}$-plane due to a non-zero net circulation Γ_o around the circular cylinder is equal to

$$\tilde{w}^o(\tilde{z}) = -\frac{\mathrm{i}\Gamma_o}{2\pi}\log(\tilde{z} - \tilde{z}_o). \tag{21}$$

https://doi.org/10.1017/S0022112008000359 Published online by Cambridge University Press

By virtue of (13), (15) and (20–21), we obtain

$$w(z) = w^b(z) + \sum_k -\frac{\mathrm{i}\Gamma_k}{2\pi}\left[\log\left(F(z) - F\left(z_k\right)\right) - \log\left(F(z) - F\left(z_k^I\right)\right)\right] - \frac{\mathrm{i}\Gamma_o}{2\pi}\log(F(z) - F(z_o)). \tag{22}$$

The complex velocity $\tilde{u} = \tilde{u}_{\tilde{x}} + \mathrm{i}\tilde{u}_{\tilde{y}}$ at an arbitrary point $\tilde{z}$ that does not coincide with any of the point vortices is obtained from the relation $\tilde{u}_{\tilde{x}} - \mathrm{i}\tilde{u}_{\tilde{y}} = \mathrm{d}\tilde{w}/\mathrm{d}\tilde{z}$, whereas the velocity induced at a point vortex is given by

$$\tilde{u}_{\tilde{x}} - \mathrm{i}\tilde{u}_{\tilde{y}}|_{\tilde{z}_k} = \frac{\mathrm{d}}{\mathrm{d}\tilde{z}}\left[\tilde{w} + \frac{\mathrm{i}\Gamma_k}{2\pi}\log(\tilde{z} - \tilde{z}_k)\right]_{\tilde{z}=\tilde{z}_k}. \tag{23}$$

The complex velocity at a point in the z-plane is related to that at a point in the $\tilde{z}$-plane via the chain rule in the usual way

$$u_x - \mathrm{i}u_y = \frac{\mathrm{d}w}{\mathrm{d}z} = \frac{\mathrm{d}\tilde{w}}{\mathrm{d}\tilde{z}}\frac{\mathrm{d}F}{\mathrm{d}z}. \tag{24}$$

This relation is true everywhere except at the vortex locations where, due to a theorem by Lin (1941*b*), we have

$$u_x - \mathrm{i}u_y\,|_{z_k} = \frac{\mathrm{d}}{\mathrm{d}z}\left[w(z) - \frac{\mathrm{i}\Gamma_k}{4\pi}\log\left(\frac{\mathrm{d}F}{\mathrm{d}z}\right)\right]_{z=z_k}. \tag{25}$$

Lin (1941*a*) showed that there exists a Kirchhoff–Routh function $W = W(x_1, y_1, \ldots, x_n, y_n)$ such that the motion of the kth vortex is given by

$$\Gamma_k u_k = \left(\frac{\partial W}{\partial y_k}, -\frac{\partial W}{\partial x_k}\right)^T. \tag{26}$$

Here, $u_k = (u_x, u_y)^T|_{(x_k, y_k)}$ denotes the ordinary fluid velocity of the kth vortex. Lin also investigated the behaviour of the Kirchhoff–Routh function under a conformal transformation in Lin (1941*b*) where he showed that the transformed function is given by

$$W(x_1, y_1, \ldots, x_n, y_n) = \tilde{W}(\tilde{x}_1, \tilde{y}_1, \ldots, \tilde{x}_n, \tilde{y}_n) - \sum_{k=1}^{n}\frac{\Gamma_k^2}{4\pi}\log\left|\frac{\mathrm{d}F}{\mathrm{d}z}\right|_{z_k}. \tag{27}$$

By definition, the Kirchhoff–Routh function in the circle-plane is equal to

$$\tilde{W} = \sum_k \Gamma_k\tilde{\psi}^b(\tilde{z}_k) + \sum_{k,l,k\neq l} -\frac{\mathrm{i}\Gamma_k\Gamma_l}{4\pi}\left[\log|\tilde{z}_l - \tilde{z}_k| - \log\left|\tilde{z}_l - \tilde{z}_k^I\right|\right] + \sum_k \frac{\mathrm{i}\Gamma_k^2}{4\pi}\log\left|\tilde{z}_k - \tilde{z}_k^I\right| + \sum_k -\frac{\mathrm{i}\Gamma_k\Gamma_o}{2\pi}\log|\tilde{z}_k - \tilde{z}_o|, \tag{28}$$

which can be expressed in the z-plane by substituting (28) into (27) and using (13).

The Kirchhoff–Routh theory remains valid when the function W is expressed in terms of the body-fixed coordinates (X_k, Y_k). Namely, we have

$$\Gamma_k\left(\frac{\mathrm{d}\boldsymbol{X}_k}{\mathrm{d}t} + \boldsymbol{\Omega}\times\boldsymbol{X}_k + \boldsymbol{V}\right) = \frac{\partial W}{\partial Y_k}\boldsymbol{b}_1 - \frac{\partial W}{\partial X_k}\boldsymbol{b}_2. \tag{29}$$

To obtain W in terms of the body coordinates (X_k, Y_k), it suffices to use ψ^b from (19), rewrite (20) and (21) in terms of the body coordinates $\tilde{Z}$ and use the conformal

https://doi.org/10.1017/S0022112008000359 Published online by Cambridge University Press

transformation $\tilde{Z} = F(Z)$. To this end, $W(X_1, Y_1, \ldots, X_N, Y_N)$ in the body frame reads as

$$W = \sum_k \Gamma_k \psi^b(Z_k) + \sum_{k,l(k\neq l)} -\frac{\Gamma_k \Gamma_l}{4\pi}\left(\log|F(Z_k) - F(Z_l)| - \log\left|F(z_k) - \frac{1}{F^*(Z_l)}\right|\right)$$

$$+ \sum_k \frac{\Gamma_k^2}{4\pi}\log\left|F(Z_k) - \frac{1}{F^*(Z_k)}\right| + \sum_k -\frac{\Gamma_k \Gamma_o}{2\pi}\log|F(Z_k)| - \sum_k \frac{\Gamma_k^2}{4\pi}\log\left|\frac{\mathrm{d}F}{\mathrm{d}Z}\right|_{Z_k}. \quad (30)$$

5. Equations of motion

Let $\boldsymbol{p}_{fluid}$ and π_{fluid} be the linear and angular impulse of the fluid with respect to the inertial frame $\{\boldsymbol{e}_i\}$. Following a similar derivation to that in Saffman (1992) and Shashikanth *et al.* (2002) and normalizing the fluid density to one, we can readily verify that the fluid impulse due to the body with circulation and the point vortices is

$$\boldsymbol{p}_{fluid} = \oint_{\partial\mathscr{B}} \phi^b \boldsymbol{n}\,\mathrm{d}s + \oint_{\partial\mathscr{B}} \boldsymbol{x} \times (\boldsymbol{n} \times \boldsymbol{u}^v)\,\mathrm{d}s + \sum_k \Gamma_k \boldsymbol{x}_k \times \boldsymbol{e}_3 + \Gamma_o \boldsymbol{x}_o \times \boldsymbol{e}_3, \quad (31a)$$

$$\boldsymbol{\pi}_{fluid} = \oint_{\partial\mathscr{B}} \phi^b \boldsymbol{x} \times \boldsymbol{n}\,\mathrm{d}s - \tfrac{1}{2}\oint_{\partial\mathscr{B}} \|\boldsymbol{x}\|^2 \boldsymbol{n} \times \boldsymbol{u}^v\,\mathrm{d}s - \tfrac{1}{2}\sum_k \Gamma_k \|\boldsymbol{x}_k\|^2 \boldsymbol{e}_3 - \tfrac{1}{2}\Gamma_o \|\boldsymbol{x}_o\|^2 \boldsymbol{e}_3, \quad (31b)$$

where $\boldsymbol{u}^v = (\partial\psi^v/\partial y)\boldsymbol{e}_1 - (\partial\psi^v/\partial x)\boldsymbol{e}_2$ denotes the velocity induced by the point vortices at the solid boundary and $\boldsymbol{x}_o$ corresponds to the conformal centre z_o – the conformal centre has the property that the moment due to a net circulation about $\boldsymbol{x}_o$ is zero ($\boldsymbol{x}_o$ can also be thought of as the centroid of vorticity, or image vorticity). The total impulse of the solid–fluid system is equal to

$$\boldsymbol{p} = m\boldsymbol{v} + \boldsymbol{p}_{fluid}, \qquad \boldsymbol{\pi} = I\dot{\beta}\,\boldsymbol{e}_3 + \boldsymbol{x}_o \times m\boldsymbol{v} + \boldsymbol{\pi}_{fluid}, \quad (32)$$

where m and I are the mass and moment of inertia of the solid body. In the absence of external forces and moments applied to the solid–fluid system, the total linear and angular impulse are conserved,

$$\dot{\boldsymbol{p}} = 0, \qquad \dot{\boldsymbol{\pi}} = 0. \quad (33)$$

Expressions for the linear and angular impulse with respect to the body–frame can be readily computed by transforming (31) and (32) to the body frame. It is convenient for what follows to introduce the components of the impulse $\boldsymbol{P}^b$ and $\boldsymbol{\Pi}^b$ due to the motion of the solid body

$$\boldsymbol{P}^b = m\boldsymbol{V} + \oint_{\partial\mathscr{B}} \phi^b \boldsymbol{N}\,\mathrm{d}s, \qquad \boldsymbol{\Pi}^b = I\boldsymbol{\Omega} - \tfrac{1}{2}\oint_{\partial\mathscr{B}} \phi^b \boldsymbol{X} \times \boldsymbol{N}\,\mathrm{d}s, \quad (34)$$

and the impulse components $\boldsymbol{P}^v$ and $\boldsymbol{\Pi}^v$ due to the presence of the point vortices

$$\boldsymbol{P}^v = \oint_{\partial\mathscr{B}} \boldsymbol{X} \times (\boldsymbol{N} \times \boldsymbol{U}^v)\,\mathrm{d}s + \sum_k \Gamma_k \boldsymbol{X}_k \times \boldsymbol{b}_3, \quad (35a)$$

$$\boldsymbol{\Pi}^v = -\frac{1}{2}\oint_{\partial\mathscr{B}} \|\boldsymbol{X}\|^2 \boldsymbol{N} \times \boldsymbol{U}^v\,\mathrm{d}s - \tfrac{1}{2}\sum_k \Gamma_k \|\boldsymbol{X}_k\|^2 \boldsymbol{b}_3. \quad (35b)$$

Here, $\boldsymbol{N}$ and $\boldsymbol{U}^v$ denote the normal vector and fluid velocity expressed in body frame.

https://doi.org/10.1017/S0022112008000359 Published online by Cambridge University Press

The impulse $\boldsymbol{P}^b$ and $\boldsymbol{\Pi}^b$ from (34) can be conveniently written, following a standard procedure (see e.g. Kanso *et al.* 2005), as follows

$$\begin{pmatrix} \boldsymbol{\Pi}^b \\ \boldsymbol{P}^b \end{pmatrix} = \mathbb{I} \begin{pmatrix} \boldsymbol{\Omega} \\ \boldsymbol{V} \end{pmatrix}. \tag{36}$$

Here, $\mathbb{I}$ is an inertia matrix that is the sum of the actual body inertia $\mathbb{I}^b$ and the added inertias $\mathbb{I}^a$

$$\mathbb{I}^b = \begin{pmatrix} I & 0 & 0 \\ 0 & m & 0 \\ 0 & 0 & m \end{pmatrix}, \quad \mathbb{I}^a = \begin{pmatrix} \oint \varphi_\Omega \dfrac{\partial \varphi_\Omega}{\partial n}\,\mathrm{d}s & \oint \varphi_\Omega \dfrac{\partial \varphi_1}{\partial n}\,\mathrm{d}s & \oint \varphi_\Omega \dfrac{\partial \varphi_2}{\partial n}\,\mathrm{d}s \\ \oint \varphi_1 \dfrac{\partial \varphi_\Omega}{\partial n}\,\mathrm{d}s & \oint \varphi_1 \dfrac{\partial \varphi_1}{\partial n}\,\mathrm{d}s & \oint \varphi_1 \dfrac{\partial \varphi_2}{\partial n}\,\mathrm{d}s \\ \oint \varphi_2 \dfrac{\partial \varphi_\Omega}{\partial n}\,\mathrm{d}s & \oint \varphi_2 \dfrac{\partial \varphi_1}{\partial n}\,\mathrm{d}s & \oint \varphi_2 \dfrac{\partial \varphi_2}{\partial n}\,\mathrm{d}s \end{pmatrix}. \tag{37}$$

Meanwhile, $\boldsymbol{P}^v$ and $\boldsymbol{\Pi}^v$ of (35) can be simplified further by proving, following Shashikanth (2005), that

$$\oint_{\partial \mathscr{B}} \boldsymbol{X} \times (\boldsymbol{N} \times \boldsymbol{U}^v)\,\mathrm{d}s = \sum_k \Gamma_k \psi_1(\boldsymbol{X}_k)\,\boldsymbol{b}_1 + \sum_k \Gamma_k \psi_2(\boldsymbol{X}_k)\,\boldsymbol{b}_2, \tag{38}$$

and

$$-\tfrac{1}{2} \oint_{\partial \mathscr{B}} \|\boldsymbol{X}\|^2 \boldsymbol{N} \times \boldsymbol{U}^v\,\mathrm{d}s = \sum_k \Gamma_k \psi_\Omega(\boldsymbol{X}_k)\,\boldsymbol{b}_3. \tag{39}$$

Hence, (35a, b) become

$$\boldsymbol{P}^v = \sum_k \Gamma_k \psi_1(\boldsymbol{X}_k)\,\boldsymbol{b}_1 + \sum_k \Gamma_k \psi_2(\boldsymbol{X}_k)\,\boldsymbol{b}_2 \; + \; \sum_k \Gamma_k \boldsymbol{X}_k \times \boldsymbol{b}_3, \tag{40a}$$

$$\boldsymbol{\Pi}^v = \left(\sum_k \Gamma_k \psi_\Omega(\boldsymbol{X}_k) \; - \; \tfrac{1}{2} \sum_k \Gamma_k \|\boldsymbol{X}_k\|^2 \right) \boldsymbol{b}_3. \tag{40b}$$

Define the linear and angular impulse $\boldsymbol{P} = \boldsymbol{P}^b + \boldsymbol{P}^v$ and $\boldsymbol{\Pi} = \boldsymbol{\Pi}^b + \boldsymbol{\Pi}^v$. We can verify, using the rigid transformation (1), that $\boldsymbol{P}$ and $\boldsymbol{\Pi}$ are related to $\boldsymbol{p}$ and π in (32) as follows

$$\boldsymbol{p} = R\boldsymbol{P} + \Gamma_c\, \boldsymbol{x}_o \times \boldsymbol{e}_3, \qquad \pi = \boldsymbol{\Pi} + \boldsymbol{x}_o \times \boldsymbol{p}. \tag{41}$$

The balance laws (33) can then be expressed in the body-fixed frame in the form

$$\dot{\boldsymbol{P}} = \boldsymbol{P} \times \boldsymbol{\Omega} + \Gamma_c\, \boldsymbol{b}_3 \times \boldsymbol{V}, \qquad \dot{\boldsymbol{\Pi}} = \boldsymbol{P} \times \boldsymbol{V}. \tag{42}$$

Equations (29) and (42) form a closed system for the set of $2N + 3$ unknowns $\boldsymbol{P} = P_1\boldsymbol{b}_1 + P_2\boldsymbol{b}_2$, $\boldsymbol{\Pi} = \Pi\,\boldsymbol{b}_3$ and $\boldsymbol{X}_k = X_k\boldsymbol{b}_1 + Y_k\boldsymbol{b}_2$. The body orientation and the position of the conformal centre (origin of body-fixed frame) can be found by integrating $\dot{\beta} = \Omega$ and $\dot{\boldsymbol{x}}_o = R\boldsymbol{V}$.

Remark 1. It is worth emphasizing that $\boldsymbol{p}$ and π are conserved quantities while $\boldsymbol{P}$ and $\boldsymbol{\Pi}$ are not. However, the system (29) and (42) may admit integrals of motion (i.e. functions of $(\boldsymbol{\Pi}, \boldsymbol{P}, \boldsymbol{X}_k)$ that are conserved). An example of such functions for $\Gamma_c = 0$ is $C = \|\boldsymbol{P}\|^2$. In the case when Γ_c is not zero, $\|\boldsymbol{P}\|^2$ may no longer be conserved, but we can construct the following integral of motion

$$C = \tfrac{1}{2}\|\boldsymbol{P}\|^2 + \Gamma_c\, \boldsymbol{\Pi}. \tag{43}$$

https://doi.org/10.1017/S0022112008000359 Published online by Cambridge University Press

Remark 2. The system of equations (42) and (29) is a Lie–Poisson system whose Hamiltonian structure is discussed in Shashikanth (2005) for the case $\Gamma_o = 0$ and in Borisov *et al.* (2007) for the general case considered here.

6. An elliptic cylinder interacting with vortex pairs

Consider a cylinder with an elliptic cross-section interacting with pairs of point vortices of equal and opposite strength. Assume that the circulation around the ellipse is zero, $\Gamma_o = 0$. Let a and b be the major and minor axes of the ellipse. The conformal transformation $\tilde{Z} = F(Z)$ that maps the exterior of the ellipse to the exterior of the unit circle can be conveniently described by introducing hyperbolic coordinates (μ, ν),

$$Z = c\cosh(\mu + \mathrm{i}\nu) = c\cosh\mu\cos\nu + \mathrm{i}c\sinh\mu\sin\nu, \qquad c^2 = a^2 - b^2, \tag{44}$$

so that

$$\tilde{Z} = F(Z) = (a-b)\mathrm{e}^{\mu+\mathrm{i}\nu}. \tag{45}$$

The complex potential $\omega^b(Z) = \phi^b + \mathrm{i}\psi^b$ of (19) can be expressed in hyperbolic coordinates as (see e.g. Batchelor 1970, or Lamb 1932)

$$w^b = -V_1\, b\sqrt{\frac{a+b}{a-b}}\mathrm{e}^{-(\mu+\mathrm{i}\nu)} - \mathrm{i}\,V_2\, a\sqrt{\frac{a+b}{a-b}}\mathrm{e}^{-(\mu+\mathrm{i}\nu)} - \mathrm{i}\,\Omega\left(\frac{a+b}{2}\right)^2\mathrm{e}^{-2(\mu+\mathrm{i}\nu)}. \tag{46}$$

To this end, we can readily verify that the inertia matrices of (37) are given by

$$\mathbb{I}^b = \begin{pmatrix} \frac{1}{4}\pi ab(a^2+b^2) & 0 & 0 \\ 0 & \pi ab & 0 \\ 0 & 0 & \pi ab \end{pmatrix} \qquad \mathbb{I}^a = \begin{pmatrix} \frac{1}{8}\pi(a^2-b^2)^2 & 0 & 0 \\ 0 & \pi b^2 & 0 \\ 0 & 0 & \pi a^2 \end{pmatrix}. \tag{47}$$

The complex potential ω and the Kirchhoff–Routh function W of (30) in the Z-plane can both be expressed, by virtue of (45) and after some standard algebraic manipulations, in terms of the hyperbolic variables μ_k and ν_k. The expressions for the stream and Kirchhoff–Routh functions are substituted into (29) and (42) to obtain equations for (X_k, Y_k) and (Π, P_1, P_2).

6.1. *Relative equilibria and their stability*

We distinguish two families of relative equilibria for the problem of an ellipse interacting dynamically with a vortex pair (figure 2). By relative equilibria, we mean solutions of (29) and (42) where the point vortices move rigidly (at the same velocity) with the cylinder and are stationary in the body frame. The first family of equilibria will be referred to as the moving Föppl equilibria since it is a generalization of the classical Föppl equilibria behind a stationary circular cylinder in an ambient uniform flow. It was discussed in Shashikanth *et al.* (2002) for the case of a moving circular cylinder. A study of the classical equilibria behind a stationary elliptic cylinder can be found in Hill (1998). Similar results hold for the moving elliptic cylinder. The positions Z_{e1} of the moving Föppl equilibria are located on the images (under the conformal transformation) of the curves $\tilde{Z}_{e1} = \tilde{R}_{e1}\exp^{\pm\mathrm{i}\tilde{\theta}_{e1}}$ described by

$$\sin^2(\tilde{\theta}_{e1}) = \frac{(\alpha^2-1)^2(\alpha^2-\lambda)}{4(\alpha^6-\lambda)}, \qquad \alpha = \tilde{R}_{e1}, \qquad \lambda = \frac{a-b}{a+b}. \tag{48}$$

https://doi.org/10.1017/S0022112008000359 Published online by Cambridge University Press

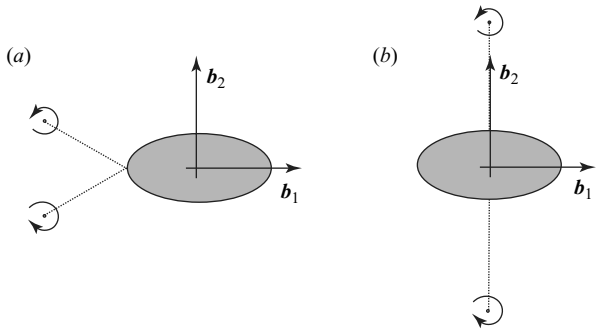


FIGURE 2. Relative equilibria where the vortices (of equal and opposite strength) and the ellipse are moving rigidly (with the same velocity) in the $\boldsymbol{b}_1$-direction: (*a*) moving Föppl equilibrium and (*b*) relative equilibrium where the vortices are located on the $\boldsymbol{b}_2$ axis of symmetry.

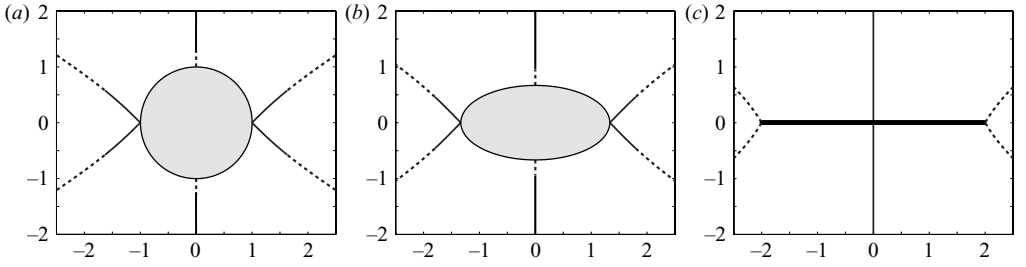


FIGURE 3. The loci of the relative equilibria associated with a translational rigid motion in the $\boldsymbol{b}_1$-direction. Both the moving Föppl equilibria and the relative equilibria located on the axis of symmetry are depicted in (*a*) for a circular cylinder with aspect ratio $b/a = 1$, (*b*) for an elliptic cylinder with $b/a = 0.5$, and (*c*) for a flat plate with $b/a = 0$. The stability of these equilibria depends on the aspect ratio b/a of the cylinder. The region of marginal stability (subject to symmetric perturbations) is depicted by a solid line while the dashed line refer to the unstable equilibria. The instability region on the Föppl curve increases as the aspect ratio a/b decreases. At the same time, the instability region of the relative equilibria located on the ellipse axis of symmetry decreases as the aspect ratio a/b decreases.

The strength Γ_{e1} of the vortex pair is related to the velocity in the $\boldsymbol{b}_1$-direction of the vortex–ellipse system by

$$\frac{\Gamma_{e1}}{2\pi V_1} = \pm \frac{(\alpha^2-1)^2(\alpha^2+1)(\lambda-\alpha^4)^2}{\alpha(\lambda+\lambda\alpha^8-2\lambda\alpha^6-2\lambda\alpha^4+\lambda\alpha^2+\alpha^{10})} \sqrt{\frac{\alpha^2-\lambda}{\alpha^6-\lambda}}. \tag{49}$$

We find a second family of equilibria associated with a translational motion in the $\boldsymbol{b}_1$-direction. These equilibria lie along the $\boldsymbol{b}_2$-axis of symmetry of the ellipse, that is, on the line $X_{e2} = 0$. At each equilibrium position along the $\boldsymbol{b}_2$-axis, the strength of the vortex pair is related to the translational velocity of the vortex–ellipse system by

$$\frac{\Gamma_{e2}}{2\pi V_1} = \pm \frac{2(\beta^2-1)(\beta^2+1)^2(\beta^2+\lambda)}{\beta(\beta^2+1)^2(\beta^2+\lambda)+2\beta^3(1-\lambda)(\beta^2-1)}, \qquad \beta = \tilde{Y}_{e2}. \tag{50}$$

The loci of both families of relative equilibria are depicted in figure 3 for a circular cylinder with aspect ratio $b/a = 1$, an elliptic cylinder with $b/a = 0.5$, and a flat plate with $b/a = 0$.

The stability of these relative equilibria can be analysed by linearizing the set of seven equations (29) and (42) about the equilibrium positions and computing the

https://doi.org/10.1017/S0022112008000359 Published online by Cambridge University Press

eigenvalues of the associated Jacobian matrix. Because the system (29) and (42) is Hamiltonian, we can expect only to deduce marginal stability (eigenvalues of the linearized system lie on the imaginary axis) or instability. To confirm stability subject to finite perturbations, we must conduct a nonlinear stability analysis in the Lyapunov sense. It is important to note that Shashikanth *et al.* (2002) studied the linear and nonlinear stability of the moving Föppl equilibria behind a circular cylinder. The linear stability analysis that we present here differs from in Shashikanth *et al.* (2002) in two ways. First, the space of the dynamics of the ellipse–vortex system is one-dimension larger than the circle–vortex system owing to the presence of the rotational momentum Π. Secondly, the existence and stability of the family of relative equilibria located at $X_{e2} = 0$ was not mentioned in Shashikanth *et al.* (2002).

Equations (29) and (42) and their linearized version about the equilibrium positions can be written, respectively, in the form

$$\frac{\mathrm{d}}{\mathrm{d}t}\begin{pmatrix} X_1 \\ Y_1 \\ X_2 \\ Y_2 \\ P_1 \\ P_2 \\ \Pi \end{pmatrix} = \boldsymbol{F}(X_1, Y_1, X_2, Y_2, P_1, P_2, \Pi), \qquad \frac{\mathrm{d}}{\mathrm{d}t}\begin{pmatrix} \delta X_1 \\ \delta Y_1 \\ \delta X_2 \\ \delta Y_2 \\ \delta P_1 \\ \delta P_2 \\ \delta \Pi \end{pmatrix} = D\begin{pmatrix} \delta X_1 \\ \delta Y_1 \\ \delta X_2 \\ \delta Y_2 \\ \delta P_1 \\ \delta P_2 \\ \delta \Pi \end{pmatrix}, \tag{51}$$

where $\boldsymbol{F}$ is a (seven-dimensional) vector-valued function given by the right-hand side of (29) and (42) and $\boldsymbol{D} = \nabla \boldsymbol{F}$ is the 7×7 Jacobian matrix evaluated at the equilibria $e1$ and $e2$. The δ denotes infinitesimal perturbations. The matrix $\boldsymbol{D}$ is computed numerically using centered differences.

We first examine the eigenvalues of $\boldsymbol{D}$ for the family of moving Föppl equilibria. We can verify numerically that, analogously to the Föppl equilibria behind a moving circular cylinder, the linearized equations in (51) decouple under symmetric and antisymmetric perturbations of the form

$$\delta X_1 = \delta X_s, \quad \delta Y_1 = \delta Y_s, \quad \delta X_2 = \delta X_s, \quad \delta Y_2 = -\delta Y_s, \quad \delta P_1, \quad \delta P_2 = 0, \quad \delta \Pi = 0, \tag{52}$$

and

$$\delta X_1 = \delta X_a, \quad \delta Y_1 = \delta Y_a, \quad \delta X_2 = -\delta X_a, \quad \delta Y_2 = \delta Y_a, \quad \delta P_1 = 0, \quad \delta P_2, \quad \delta \Pi. \tag{53}$$

An arbitrary perturbation can be written in terms of the symmetric perturbation $(\delta X_s, \delta Y_s, \delta P_1)$ and the antisymmetric perturbation $(\delta X_a, \delta Y_a, \delta P_2, \delta \Pi)$ in the straightforward manner

$$\left.\begin{aligned} &\delta X_1 = \delta X_s + \delta X_a, \quad \delta Y_1 = \delta Y_s + \delta Y_a, \\ &\delta X_2 = \delta X_s - \delta X_a, \quad \delta Y_2 = -\delta Y_s + \delta Y_a, \\ &\delta P_1 = \delta P_1 + 0, \quad \delta P_2 = 0 + \delta P_2, \quad \delta \Pi = 0 + \delta \Pi. \end{aligned}\right\} \tag{54}$$

These relations define a non-singular transformation from $(\delta X_1, \delta Y_1, \delta X_2, \delta Y_2, \delta P_1, \delta P_2, \delta \Pi)$ to the vector $(\delta X_s, \delta Y_s, \delta P_1, \delta X_a, \delta Y_a, \delta P_2, \delta \Pi)$. The linearized equations in (51) can be rewritten in terms of the vector of symmetric and antisymmetric

https://doi.org/10.1017/S0022112008000359 Published online by Cambridge University Press

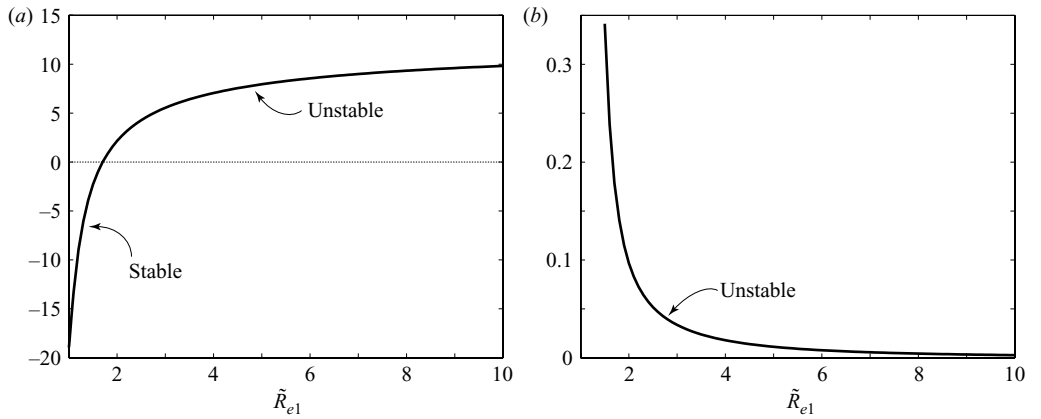


FIGURE 4. Plots of the eigenvalues corresponding to the moving Föppl equilibria as a function of the position along the Föppl curve. The square of the non-zero eigenvalue of D_s is plotted in (a) while the maximum eigenvalue of D_a is plotted in (b). The ellipse parameters are set to $a = 4/3$ and $b = 2/3$, the vortex strength is set to $\Gamma_{e1} = \pm 1$.

pertubations

$$\frac{\mathrm{d}}{\mathrm{d}t}\begin{pmatrix} \delta X_s \\ \delta Y_s \\ \delta P_1 \\ \delta X_a \\ \delta Y_a \\ \delta P_2 \\ \delta \Pi \end{pmatrix} = \begin{pmatrix} D_{s_{3\times 3}} & 0_{3\times 4} \\ 0_{4\times 3} & D_{a_{4\times 4}} \end{pmatrix} \begin{pmatrix} \delta X_s \\ \delta Y_s \\ \delta P_1 \\ \delta X_a \\ \delta Y_a \\ \delta P_2 \\ \delta \Pi \end{pmatrix}. \tag{55}$$

We find, upon numerically computing the eigenvalues of D_s and D_a that these moving Föppl equilibria are unstable under antisymmetric perturbations, whereas there exists a small region on the Föppl curve where these equilibria are marginally stable under symmetric perturbations. Figure 4 shows a plot of the square of the non-zero eigenvalue of D_s and a plot of the maximum eigenvalue of D_a for the ellipse parameters $a = 4/3$ and $b = 2/3$. This result is consistent with that of the moving the Föppl equilibria behind a moving circular cylinder.

We now examine the eigenvalues of D for the family of equilibria located at $X_{e2} = 0$. We can verify numerically that the linearized equations in (51) also decouple under the symmetric and antisymmetric perturbations $(\delta X_s, \delta Y_s, \delta P_1)$ and $(\delta X_a, \delta Y_a, \delta P_2, \delta \Pi)$ as in (52–55). We Find, upon numerically computing the eigenvalues of D_s and D_a, that these equilibria are unstable under antisymmetric perturbations, whereas they are marginally stable under symmetric perturbations apart from a small region close to the ellipse in which they are unstable. Figure 5 gives a plot of the square of the non-zero eigenvalue of D_s and a plot of the square of the eigenvalues of D_a for the ellipse parameters $a = 4/3$ and $b = 2/3$. This result differs significantly from the stability of the classical equilibria in the case of a stationary ellipse. In the classical case, instability occurs under symmetric perturbations for all such equilibria perhaps owing to artificially maintaining a constant free-stream velocity while perturbing the positions of the point vortices.

In the case of symmetric perturbations, the region of marginal stability for both the Föppl equilibria and the equilibria on $X_{e2} = 0$ depend on the aspect ratio b/a as pointed out in figure 3. We define the critical values α_c and β_c as those for which

https://doi.org/10.1017/S0022112008000359 Published online by Cambridge University Press

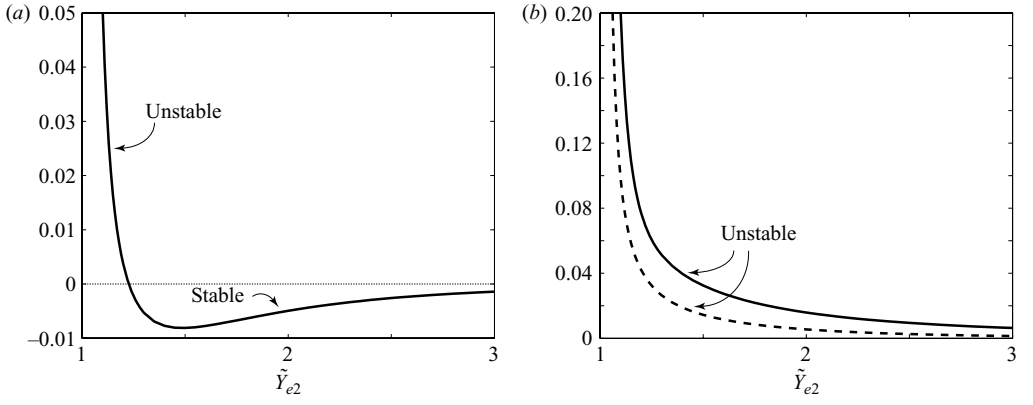


FIGURE 5. Plots of the eigenvalues corresponding to the relative equilibria located at the axis of symmetry as a function of $\tilde{Y}_{e2}$. The square of the non-zero eigenvalue of D_s are plotted in (a) while the square of the eigenvalues of D_a (one has two pairs of complex eigenvalues) are plotted in (b). The ellipse parameters are set to $a = 4/3$ and $b = 2/3$, the vortex strength is set to $\Gamma_{e2} = \pm 1$.

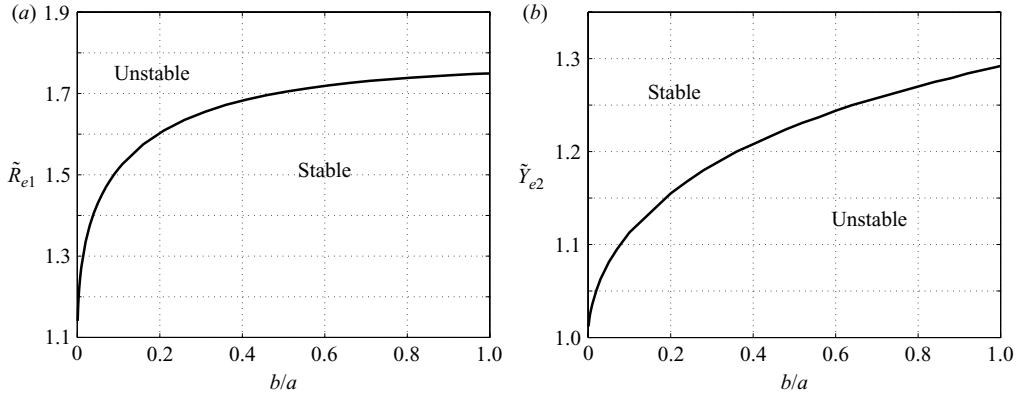


FIGURE 6. The critical position α_c is plotted as a function of the aspect ratio b/a in (a) and the critical position β_c is plotted versus b/a in (b). The critical values α_c and β_c are defined as those for which the linear stability subject to symmetric perturbations changes character. That is, the moving Föppl equilibria are marginally stable for $\alpha < \alpha_c$ and unstable for $\alpha > \alpha_c$ whereas the relative equilibria along $X_{e2} = 0$ are unstable for $\beta < \beta_c$ and are marginally stable for $\beta > \beta_c$. As noted in figure 3, as b/a descreases, the region of instability increases for the moving Föppl equilibria while the region of instability decreases for the equilibria located at $X_{e2} = 0$. The vortex strength is set to $\Gamma_{e1} = \Gamma_{e2} = \pm 1$.

the linear stability subject to symmetric perturbations changes character. That is, α_c is defined such that a moving Föppl equilibrium is marginally stable if $\alpha < \alpha_c$ and unstable if $\alpha > \alpha_c$. Meanwhile, β_c is defined such that a relative equilibrium along $X_{e2} = 0$ is marginally stable if $\beta > \beta_c$ and unstable if $\beta < \beta_c$. The critical positions α_c and β_c are plotted in figure 6 as a function of the aspect ratio b/a. We find that as we flatten the elliptic body, that is, as we decrease b/a while keeping $(a + b)/2 = 1$, the stability region along the Föppl curves decreases whereas the stability region along the axis of symmetry increases.

The marginal stability deduced from this linear analysis does not guarantee stability subject to finite perturbations. Here, we provide only numerical evidence that these

https://doi.org/10.1017/S0022112008000359 Published online by Cambridge University Press

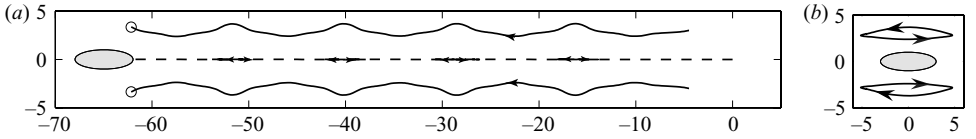


FIGURE 7. The motion of the cylinder and a vortex pair in (*a*) inertial frame and (*b*) body frame. The parameter values are set at $a=3$, $b=1$, $\Gamma_1=-10$, $\Gamma_2=10$. The point vortices are initially located at $Z_1(0)=-4.5+\mathrm{i}3$, $Z_2(0)=-4.5-\mathrm{i}3$, while the ellipse is initially placed at $(0, 0)$ with zero initial velocity and zero orientation. The integration time is 200.

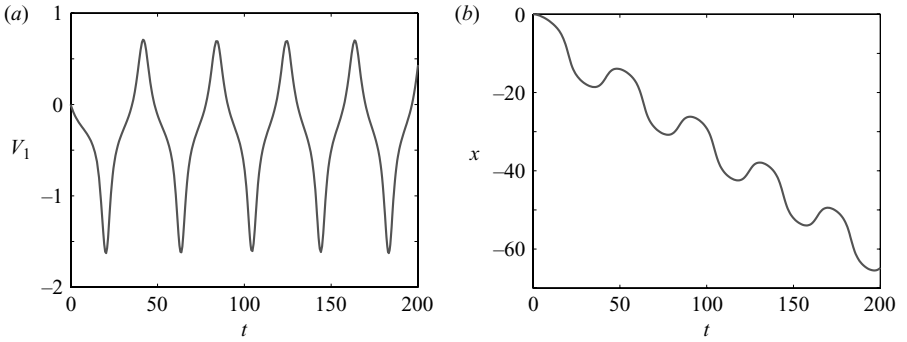


FIGURE 8. Motion versus time: (*a*) ellipse velocity and (*b*) its position correspond to the motion shown in figure 7.

marginally stable equilibria are indeed nonlinearly stable, as indicated in figure 7(*b*). To confirm stability subject to finite perturbations, we would need to conduct a nonlinear stability analysis which is beyond the scope of this paper.

6.2. *Application to swimming*

These unstable and stable equilibria may be exploited to design swimming motions of the ellipse. In this section, we investigate some trajectories close to the relative equilibria and their relation to swimming motions by numerically integrating (29) and (42).

Figure 7 shows the motion of the cylinder and a vortex pair both in body-fixed and inertial frame. Plots of the cylinder's velocity and position versus time are shown in figure 8. The parameter values are set at $a=3$, $b=1$, $\Gamma_1=-10$, $\Gamma_2=10$. The point vortices are initially located at $Z_1(0)=-4.5+\mathrm{i}3$, $Z_2(0)=-4.5-\mathrm{i}3$, while the ellipse is initially placed at $(0, 0)$ with zero initial velocity and zero orientation. The integration time is 200. The initial conditions can be thought of as a finite perturbation from the equilibria at $X_{e2}=0$, yet the point vortices trace closed trajectories in body frame (figure 7*b*) – this behaviour is typical around a stable equilibrium. We observed similar behaviour for a wide range of initial conditions which suggests that the equilibria at $X_{e2}=0$ are stable to finite perturbations.

In figure 7, the ellipse starts moving in the same direction as the vortex pair, reaches zero velocity, reverses its direction of motion, reaches zero velocity again then returns to moving in the same direction as the vortex pair. This behaviour is repeated periodically. This trajectory consists of both *following* and *swimming* motions. By following, we mean when the vortices and the body move in the same direction following each other (the relative equilibria are examples of following motions). By swimming, we mean when the body moves in the direction opposite to the motion of

https://doi.org/10.1017/S0022112008000359 Published online by Cambridge University Press

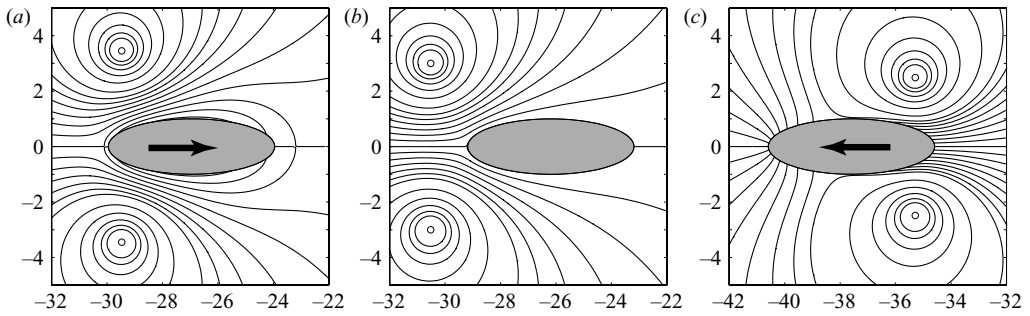


FIGURE 9. Snapshots of the streamlines at three different times taken from the trajectory depicted in figure 7. (*a*) A plot of the streamlines at time $t = 86.62$. The ellipse is moving in the direction opposite to the point vortices with velocity $V_1 = +0.4586$. Clearly, there exist two stagnation points in the flow around the ellipse. (*b*) A plot of the streamlines at time $t = 90.87$ where the ellipse's velocity is almost zero. The instantaneous stagnation point lies at the boundary of the ellipse. (*c*) A plot of the streamlines at $t = 106.65$ at which the ellipse is moving with velocity $V_1 = -1.1824$ in the same direction as the point vortices and there are no stagnation points outside the solid body.

the vortices themselves. Such swimming motions are characterized by an instantaneous stagnation point in the flow between the body and the vortices. If we understand how to create such stagnation points in the flow by perturbing from a relative equilibrium, we could exploit the relative equilibria to design swimming trajectories. Snapshots of the streamlines at three different times are depicted in figure 9. In figure 9(*a*) is a plot of the streamlines at time $t = 86.62$ at which the ellipse is moving in the direction opposite to the point vortices with velocity $V_1 = +0.4586$. Clearly, there exist two stagnation points in the flow around the ellipse. Figure 9(*b*) is a plot of the streamlines at time $t = 90.87$ where the ellipse's velocity is almost zero. The instantaneous stagnation point lies at the boundary of the ellipse. Figure 9(*c*) is a plot of the streamlines at $t = 106.65$ at which the ellipse is moving with velocity $V_1 = -1.1824$ in the same direction as the point vortices. This behaviour reminds as of the leapfrogging of vortex rings considered in Shashikanth & Marsden (2003). The vortex pair and its image vorticity may be thought of as a pair of vortex rings subject to the constraint that the boundary of the solid is a streamline – this analogy remains to be investigated.

A similar behaviour is observed in figure 10 which depicts the motion of the cylinder and two vortex pairs in inertial frame. The parameter values are set at $a = 3$, $b = 1$, $\Gamma_1 = \Gamma_2 = -10$, $\Gamma_3 = \Gamma_4 = 10$, The point vortices are initially located at $Z_1(0) = -5 + \mathrm{i}10$, $Z_2(0) = 5 + \mathrm{i}10$, $Z_3(0) = -5 - \mathrm{i}10$, and $Z_4(0) = 5 - \mathrm{i}10$, while the ellipse is placed at (0, 0) with zero initial velocity and zero orientation. The integration time is 300.

The trajectories in figures 7 and 10 may be relevant for understanding the swimming of a fish in an existing vortex wake (such as that created by two neighbouring fish). As illustrated in figure 11 for three vortex pairs, by properly choosing the initial location of the vortex pairs and their strength, we could obtain a swimming motion of the body in the direction opposite to the motion of the vortex pairs. This motion reminds as of the swimming of a trout in an externally generated vortex street reported in Liao *et al.* (2003), where the fish exploits the presence of vorticity to swim upstream at a lower energy cost. In figure 11, the ellipse itself spends no energy (it does not generate any force) and its motion is due entirely to energy exploited from the presence of the

https://doi.org/10.1017/S0022112008000359 Published online by Cambridge University Press

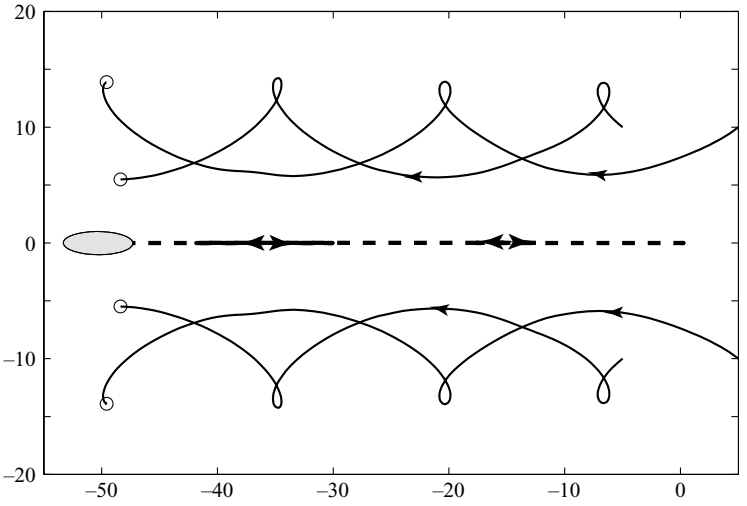


FIGURE 10. The motion of the cylinder and two vortex pairs in inertial frame. The parameter values are set at $a=3$, $b=1$, $\Gamma_1=\Gamma_2=-10$, $\Gamma_3=\Gamma_4=10$. The point vortices are initially located at $Z_1(0)=-5+\mathrm{i}10$, $Z_2(0)=5+\mathrm{i}10$, $Z_3(0)=-5-\mathrm{i}10$, and $Z_4(0)=5-\mathrm{i}10$, while the ellipse is initially placed at $(0, 0)$ with zero initial velocity and zero orientation. The integration time is 300.

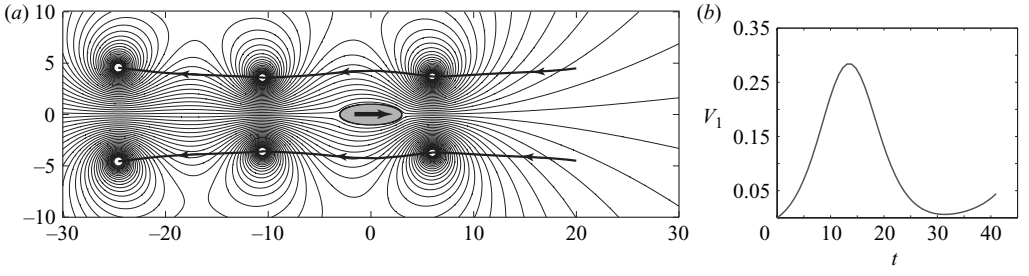


FIGURE 11. The trajectories of three vortex pairs in body-fixed frame are depicted in the solid black line. The streamlines at the end of the integration time (at $t=41$) are superimposed. The parameter values are set to $a=3$, $b=1$, $\Gamma_1=\Gamma_2=\Gamma_3=-10$, $\Gamma_4=\Gamma_5=\Gamma_6=10$, The vortex pairs are initially located at $Z_{1,4}(0)=20\pm\mathrm{i}4.5$, $Z_{2,5}(0)=6\pm\mathrm{i}3.7$, and $Z_{3,6}(0)=-10\pm\mathrm{i}3.6$, while the ellipse is initially placed at $(0, 0)$ with zero initial velocity and zero orientation. The velocity of the ellipse (b) is non-negative for all t which means that the ellipse achieves a net motion to the right while the point vortices are advected in the opposite direction. Based on this, we could propose a simple model that emulates the motion of a body in an externally generated vortex street by periodically introducing vortex pairs at the leading end of the body while periodically removing vortex pairs as they are advected far away from the body.

point vortices. Of course, this comparison is only qualitative but, inspired by these trajectories, we could propose a simple model to emulate the motion of a body in an externally generated vortex street. Consider an elliptic body (say starting at zero velocity) and place it between a number of vortex pairs, as in figure 11. Integrate in time while periodically introducing vortex pairs in the flow at the leading end of the ellipse and removing vortex pairs from the flow when they reach the other end of the ellipse. The introduction and removal of vortex pairs can be justified on physical grounds as follows. The introduction of vortex pairs emulates the vortices shed periodically by a source external to the body. The removal of vorticity after

https://doi.org/10.1017/S0022112008000359 Published online by Cambridge University Press

some time emulates the diminishing effect of the vortices on the motion of the body as they move far away from the body.

7. Summary

This paper considered the dynamics of a rigid body interacting with a finite number of point vortices in potential flow. The dynamics of the solid–fluid system was formulated in terms of the solid variables and the position of the point vortices only. The motion of the point vortices is governed by a Kirchhoff–Routh function and the equations of motion for the rigid body are derived using Newtonian mechanics. These equations were applied to the problem of an elliptic body interacting with a vortex pair. The associated relative equilibria and their stability was discussed. These models may be relevant to understanding the interaction of fish with ambient vorticity, as illustrated via numerical examples. The formulation presented here can be extended to study the interaction of point vortices with several rigid bodies in application to fish schooling. Such extension would require generalizing the work of Crowdy & Marshall (2005) which provides analytical formulae for the Kirchhoff–Routh function in multiply connected fluid domain to the case of fluid domains with moving boundaries.

The authors would like to thank Professor Paul Newton for useful comments and discussions. This work is partially supported by the National Science Foundation through the award CMMI 06-44925.

REFERENCES

Batchelor, G. K. 1970 *An Introduction to Fluid Dynamics*. Cambridge University Press.

Beal, D. N., Hover, F. S., Triantafyllou, M. S., Liao, J. C. & Lauder, G. V. 2006 Passive propulsion in vortex wakes. *J. Fluid Mech.* **549**, 385–402.

Borisov, A. V. & Mamaev, I. S. 2003 An integrability of the problem on motion of cylinder and vortex in the ideal fluid, *Regular Chaotic Dyn.* **8**, 163–166.

Borisov, A. V., Mamaev, I. S. & Ramodanov, S. M. 2007 Dynamic interaction of point vortices and a two-dimensional cylinder. *J. Math. Phy.* **48**, 1–9.

Crowdy, D. & Marshall, J. 2005 Analytical formulae for the Kirchhoff–Routh path function in multiply connected domains. *Proc. R. Soc. Lond.* A **461**, 2477–2501.

Crowdy, D. G., Surana, A. & Yick, K.-Y. 2007 The irrotational flow generated by two planar stirrers in inviscid fluid. *Phys. Fluids* **19**, 018103.

Hill, D. 1998 *Vortex Dynamics in Wake Models*. PhD thesis, California Institute of Technology.

Kanso, E., Marsden, J. E., Rowley, C. W. & Melli-Huber, J. B. 2005 Locomotion of articulated bodies in a Perfect fluid. *Intl J. Nonlinear Sci.* **15**, 255–289.

Lamb, H. 1932 *Hydrodynamics*. Dover.

Liao, J. C., Beal, D. N., Lauder, G. V. & Triantafyllou, M. S. 2003 Fish exploiting vortices decrease muscle activity. *Science* **302**, 1566–1569.

Lin, C. C. 1941*a* On the motion of vortices in two-dimensions - I. existence of the Kirchhoff–Routh function. *Proc. Natl Acad. Sci.* **27**, 570–575.

Lin, C. C. 1941*b* On the motion of vortices in two-dimensions - II. some further investigations on the Kirchhoff–Routh function. *Proc. Natl Acad. Sci.* **27**, 575–577.

Muskhelishvili, N. I. 1953 *Singular Integral Equations*. Noordhoff, Groningen, Holland.

Nair, S. & Kanso, E. 2007 Hydrodynamically coupled rigid bodies. *J. Fluid Mech.* **592**, 393–411.

Saffman, P. G. 1992, *Vortex Dynamics*. Cambridge.

Shashikanth, B. N. 2005 Poisson brackets for the dynamically interacting system of a 2D rigid cylinder and N point vortices: the case of arbitrary smooth cylinder shapes. *Regular Chaotic Dyn.* **10**, 1–10.

https://doi.org/10.1017/S0022112008000359 Published online by Cambridge University Press

Shashikanth, B. & Marsden, J. E. 2003 Leapfrogging vortex rings: Hamiltonian structure, geometric phases and discrete reduction. *Fluid Dyn. Res.* **33**, 333–356.

Shashikanth, B. N., Marsden, J. E., Burdick, J. W. & Kelly, S. D. 2002 The Hamiltonian structure of a 2D rigid circular cylinder interacting dynamically with *N* Point vortices. *Phys. Fluids* **14**, 1214–1227.

Silverman, R. 1974 *Introductory Complex Analysis*. Dover.

Wang, Q. X. 2004 Interaction of two circular cylinders in inviscid fluid. *Phys. Fluids* **16**, 4412.

https://doi.org/10.1017/S0022112008000359 Published online by Cambridge University Press